Towards expanding the optical response of Ag_2CrO_4 and Bi_2O_3 by their laser-mediated heterojunction

Rafael Omar Torres-Mendieta,[*,†] Mayara Mondego Teixeira,[‡] Gladys Mínguez-Vega,[¶] Daniele Souza,[§] Yara Galvão Gobato,[§] Héctor Beltrán-Mir,[‖] Eloisa Cordoncillo,[‖] Juan Andrés,[⊥] Miroslav Černík,[†] and Elson Longo[*,‡]

†*Institute for Nanomaterials, Advanced Technologies and Innovation, Technical University of Liberec, Studentská 1402/2, 461 17 Liberec, Czech Republic.*

‡*CDMF-UFSCar, Universidade Federal de São Carlos, P.O. Box 676, CEP, 13565-905 São Carlos-SP, Brazil.*

¶*GROC·UJI, Institut de Noves Tecnologies de la Imatge (INIT, University Jaume I (UJI), Castelló 12071, Spain.*

§*Departamento de Física, Universidade Federal de São Carlos (UFSCAR), 13565-905, São Carlos, SP, Brazil*

‖*Department of Inorganic and Organic Chemistry, University Jaume I (UJI), Castelló 12071, Spain*

⊥*Department of Analytical and Physical Chemistry, University Jaume I (UJI), Castelló 12071, Spain.*

E-mail: Rafael.Torres@tul.cz; elson.liec@gmail.com

Abstract

The formation of heterojunctions between semiconductors with distinct properties usually expands their capabilities. In this context, many methodologies have been employed in pursuing efficient and fruitful heterojunctions. However, poor attention has been paid to the employment of photonics-based strategies, which lately demonstrated to have great potential for the structural modification of semiconductors. In the current work, we report the laser-mediated generation of heterojunctions between Ag_2CrO_4 and Bi_2O_3, two semiconductors with contrasting properties. The products were prepared by the laser irradiation of different semiconductor's mixture ratios and further analyzed by various electron- and photon-based characterization techniques, differently from mechanical grinding, which is considered the most straightforward way to obtain heterojunctions. The laser's intense optical field prompted not only the formation of tight and uniform junctions between the composing semiconductors but also induced Ag and Bi nanoparticles' production on their surfaces. This resulted in a modulation of the optical band gap to the narrowest value found in the semiconductor components and low recombination of the photoinduced charge carriers regardless of the amount ratio of the composing semiconductors. Therefore, this work will be of great importance for the creation of materials with a potential exploitability in the light-powered sectors.

Introduction

The continuous endeavor for smarter solutions to the problems that our society faces results in the development of many materials with fascinating behavior. Among the virtually unlimited options available, semiconductors stand above the rest. Their study is currently shaping our times, and the clearest example of this is found in the electronic device used to consult this manuscript. The latest advances in this field, however, are not limited to the production and manipulation of the commercially available materials, but rather seek to expand their capabilities through their structural modification or interplay with dissimilar materials. Such a research path is finding in the study of heterojunctions between semiconductor/semiconductor and semiconductor/metal an escape valve that is currently leading to unprecedented results in many fields.[1–3]

In particular, the sectors related to the harvesting of the sunlight, the most widespread source of energy on the planet, are greatly benefited. Since the solar spectral irradiance finds its maximum at the visible electromagnetic spectrum range (400-800 nm),[4] the formation of heterojunctions between semiconductors is a widely used strategy to enhance the visible-light response of materials that have not the capacity of absorbing photons within such wavelength range. This leads to an enhanced separation of electron-hole pairs, suppressing their recombination, and finally enhancing their stability.[5,6] From a practical perspective, it means that heterojunctions between a material that absorbs a short fraction of the solar irradiance spectrum, and one that absorbs a wide fraction could overall improve the transformation of solar energy into charge carriers, which can be then exploited in further applications.

The strategies to manufacture such heterojunctions can encompass the employment of various sources of energy. However, a form of energy that has been poorly exploited for this is the ultrashort laser radiation. The use of such a tool can enable phenomena like ablation by plasma, which, when performed in these materials, allow their sintering and segregation of NPs;[7,8] two effects that could lead to the formation of heterojunctions when irradiating a mixture of dissimilar materials. In brief, the delivery of a large population of photons in windows of time (10^{-15}s) that are shorter than the typical electronic relaxation time (10^{-12}s), promote the multiphoton ionization of irradiated solid materials, which ends up forming a plasma of electrons above the irradiated zone. When the energy of the plasma overcomes the materials' binding one, a Coulomb explosion occurs, where their composing elements are released to the surroundings forming nanoparticles (NPs).[9,10] However, suppose this energy is extensively overpassed. In that case, a localized and excessive increment of temperature and pressure occurs. The adiabatic transfer of this energy results in the sintering and further detachment of material.[11]

Given the versatility, efficiency in NPs formation, and degree of structural modifications. In the current research work, the femtosecond laser irradiation was chosen as a tool to generate the heterojunction between Ag_2CrO_4 and Bi_2O_3; two low production cost photo-active semiconductors that, as recently discovered by our research team can be precursors for the formation of metal

NPs.[12–19] Unlike traditional strategies, this tool's use may permit not only the formation of heterojunctions, but also an additional injection of charge carriers to the material by laser-segregated metal NPs,[20] which will contribute to the expansion of the materials' capabilities.

Overall, this study serves to determine the impact that femtosecond pulsed laser radiation can have on the formation of heterojunctions, which promises to be of fundamental importance for the field since the structural changes that arise with its use can lead to more robust and complex heterojunctions.

Experimental Section

Materials

Potassium chromate (K_2CrO_4, 99.0%, Sigma-Aldrich), silver nitrate ($AgNO_3$, 99.0%, Sigma-Aldrich), and bismuth(III) oxide (Bi_2O_3, 99.9%, Sigma-Aldrich) were used as precursors.

Synthesis of Ag_2CrO_4

The Ag_2CrO_4 nanopowder was prepared through a modification of the precipitation procedure described by D. Xu and co-workers.[21] In brief, 1mM of Potassium chromate (K_2CrO_4, 99.0%, Sigma-Aldrich) was dissolved in 50 mL of distilled water (18.2 $M\Omega \cdot cm$), the solution was continuously stirred at a temperature of 60 °C. Parallelly, 2mM of silver nitrate ($AgNO_3$, 99.0%, Sigma-Aldrich) was dissolved in 50 mL of distilled water while continuously stirred at 60 °C. Once the reagents were properly dissolved, the $AgNO_3$ solution was rapidly added to the K_2CrO_4 one. After the complete addition of the $AgNO_3$ solution, the mixture became wine color and a precipitate was formed. The final mixture kept continuously stirred at 60 °C for another hour, afterward, the precipitate was washed several times with water and ethanol, the centrifuging was performed at 7000 rpm for 15 min each round and the final solid was dried in an oven at 60 °C for 24 hours.

Mixing of Ag_2CrO_4 and Bi_2O_3

Five different mixtures were selected to investigate the influence of each semiconductor in the properties of the final heterostructure. Pure Ag_2CrO_4 and Bi_2O_3, labelled as A and B, respectively, and xA-yB (x = 75, 50, 25; y = 25, 50, 75 wt%). To prepare the mixtures, the corresponding wt% of the Ag_2CrO_4 powder previously produced by precipitation and wt% of the commercial Bi_2O_3 powder were mechanically ground in an agate mortar for 15 min. Besides, the pristine Ag_2CrO_4 and Bi_2O_3 powders were also ground to simplify the structural and morphological comparisons.

Irradiation of Ag_2CrO_4 and Bi_2O_3 mixtures by femtosecond pulsed laser

The different semiconductor mixtures were irradiated by a Ti:sapphire laser (Femtopower Compact Pro, Femto Lasers) that delivers pulses at a repetition rate of 1 kHz with a width of 30 fs full width at half-maximum (FWHM), a central wavelength of 800 nm, and it has incorporated a programmable acousto-optic filter (Dazzler, Faslite) to ensure a precise pulse compression. The irradiation conditions were selected following previous studies, where the laser irradiation allowed the segregation of metal NPs out of the corresponding semiconductor matrix, which extends the possible applications for the material.[14,18] In brief, a laser beam with a mean power of 200 mW and a diameter of 6 mm at a width of $1/e^2$ was focused by a plano-convex lens with a focal length of 75 mm over the surface of the samples as it is depicted in Fig 1. The samples were first poured in the powder form over a quartz slide ($\sim$ 1.5 g), subsequently, after being pressed by another quartz slide to enable a flat surface, the corresponding sample was mounted in a motion-controlled 2D stage moving at a velocity of 0.45 mm/s in a raster pattern perpendicular to the focal plane. The irradiation conditions were fixed for all the samples, in order to compare the differences prompted by the use of the various semiconductor mixture ratios.

Every sample underwent the following irradiation cycle: after completing the irradiation in the raster pattern (one run), the samples were mixed using a spoon and then pressed again by the two quartz slides in order to be irradiated one more time (second run). Each irradiation cycle consisted of 20 runs in order to irradiate as much material as possible. After the irradiation cycles, the

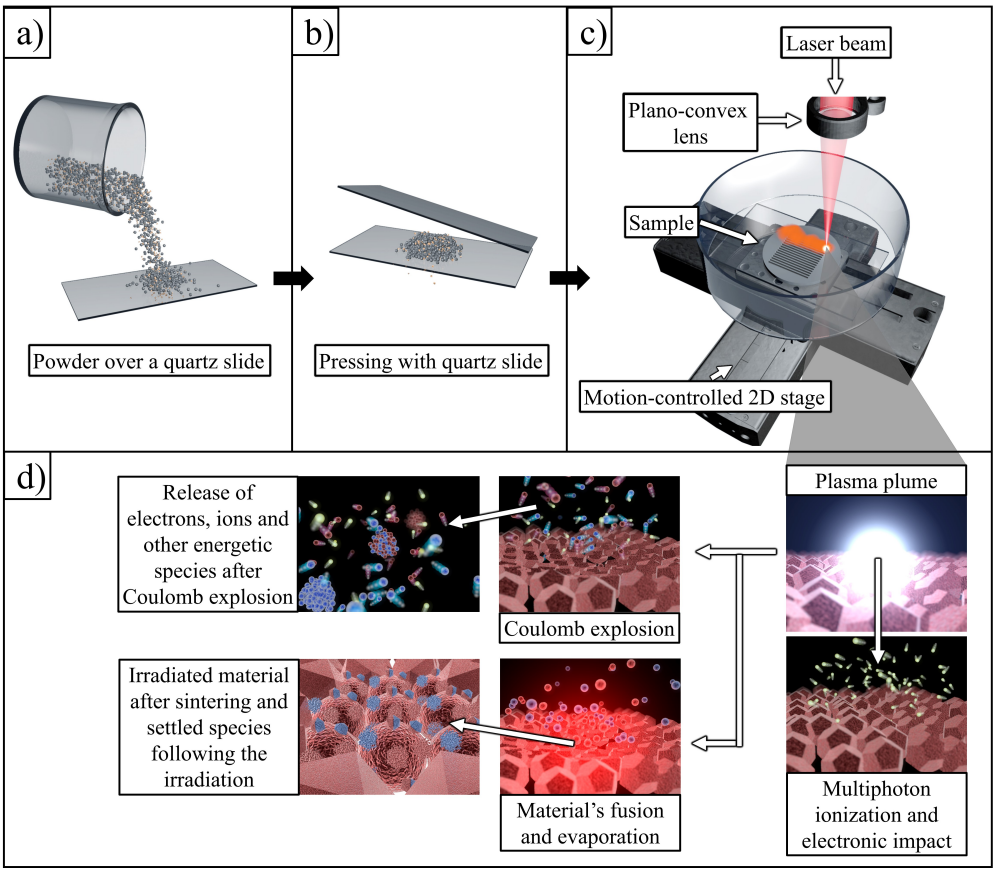

Figure 1: Scheme of the general setup and products from the laser-produced plasma: a) disposing of powder in quartz slide, b) pressing the powder with two quartz slides, c) laser irradiation while moving the sample in a raster-like pattern, and d) graphical representation of the interactions between accelerated electrons and the irradiated zone, Coulomb explosion when the plasma overpasses the material's binding energy, its products, and evaporation of material when the binding energy is severely exceeded, and the related species that arise from such interaction.

samples were collected for their further characterization.

Characterization

The samples, before and after laser irradiation, were inspected by various electron- and photon-based characterization techniques to evaluate the benefits behind the use of laser irradiation while synthesizing heterostructures from photosensitive semiconductors. The morphology of the samples was determined using a field emission gun scanning electron microscope (FEG-SEM; Supra 35-VP, Carl Zeiss) operated at 15kV. The crystalline structure of the samples was obtained by X-ray

diffraction in powder (XRD) using a diffractometer (XRD 6000, Shimadzu) operated at 30 kV. The instrument used CuKα radiation (1.5406 $\AA$), and the samples were scanned in a normal routine for 2θ ranging from 10-70° at a scanning velocity of 2°/min. The Rietveld refinement of the XRD patterns was performed using the software named "material analysis using diffraction" (MAUD).[22] The crystal structure of individual particles was obtained by high-resolution transmission electron microscopy (HR-TEM), using a transmission microscope (JEM-2100 LaB6, Jeol) operated at 200 kV. The samples' elemental distribution was assessed by a FEG-SEM (XL-30, Philips) working at 5 kV and equipped with an energy-dispersive X-ray spectroscopy (EDS) system from the Bruker brand that allows the performance of chemical microanalysis with a rapid mapping of chemical composition (EDS-Mapping).

The chemical structure and phase were determined by Raman spectroscopy using a Fourier transform Raman spectroscope (FT-Raman; RFS/100/S, Bruker), which uses as a light source a Nd:YAG nanosecond pulsed laser with a central wavelength of 1064 nm, and it is operated at a mean power of 60 mW. The FT-Raman spectra were taken in a wavenumber region from 1000-50 cm^{-1}, with a precision of 4 cm^{-1}.

The reflectance of the samples was measured by diffuse reflectance spectroscopy in the ultraviolet-visible (UV–Vis DRS) by means of a spectrophotometer (Cary 5G, Varian) working in diffusive reflectance mode, while a magnesium oxide sample holder was used as reference material. The spectra were taken in a wavelength region from 300-800 nm with a precision of 1 nm. The UV–Vis DRS spectra were later used to estimate the optical band gap energy (E_g) of the semiconductors by means of the Kubelka-Munk theory.[23] Finally, the photoluminescence (PL) spectra were obtained using a 0.5M spectrometer (500M, SPEX) coupled to a photomultiplier tube (PMT) detector and 325nm He-Cd laser excitation line with laser power of 16 mW. The PL spectra were measured in a wavelength range from 350-950 nm..

Results and discussion

Even when the simple mixing and grinding of semiconductors is considered as the most straitforward method to produce semiconductor heterojunctions, their further femtosecond pulsed laser irradiation raises a great interest because it enables the segregation of elements that compose photosensitive semiconductors. Therefore, it is expected that the laser irradiation of the investigated mixtures may enable the composition of complex structures that could present different properties than those belonging to the precursor structures.

Morphology

Fig. 2 displays significant morphological differences between the mixtures before and after being subject to laser irradiation. The largest difference between the mixtures prior to irradiation relies on the aspect of B, which after mixing with A, experiences a size reduction and shape transformation from the merged sheets into a lumpy-like structure. Moreover, when the amount of A is minimal, i.e., 25A-75B, B seems to cover the surface of A.

After the laser irradiation, it is possible to appreciate 3 different morphological alterations: (i) all the samples experience a size reduction, which correlates with the fact that the samples are being subject to an ablation phenomenon in which the material is removed out of the irradiated target to form a new structure, (ii) the edges of the non irradiated junctions get softened and in some cases the junction's components merge. As described in seminal works,[14,18] this is connected to the fact that in the ablation process, when the plasma energy greatly exceeds the binding energy of the constituent atomic clusters in the irradiated material, the temperature and pressure values can get to 1000 K and 10^{12} Pa,[24] respectively. Its interaction with the material's surface, therefore, leads to its sintering, (iii) there is segregation of NPs (Fig. 2 c)) as previously reported by our research team,[18,25] in which the femtosecond laser irradiation of Ag- and Bi-containing photosensitive semiconductors leads to the metal segregation and further NPs formation.

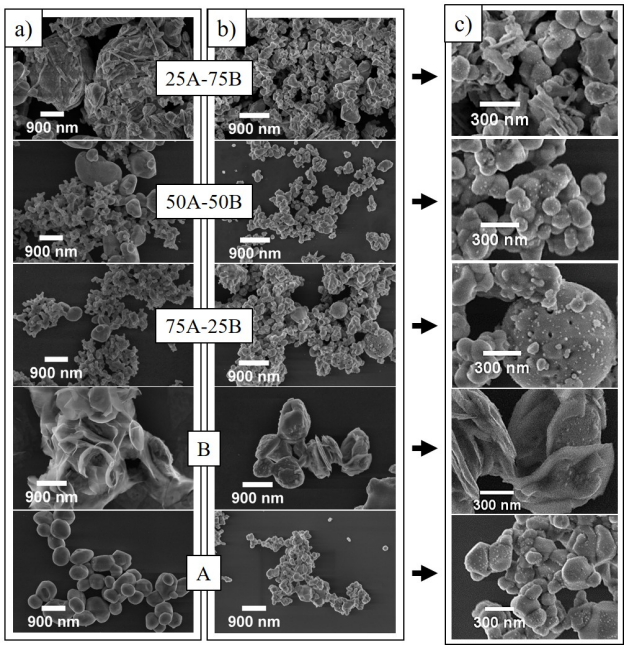

Figure 2: SEM micrographs of the different samples, a) before and b) after being subject to the femtosecond laser irradiation, and c) zoom of the irradiated samples.

Crystalline structure

Fig. 3, which displays the comparison between the XRD patterns of the samples before and after the laser irradiation, allows observing significant changes. In the case of A, its pattern can be associated with the orthorhombic crystal phase of Ag_2CrO_4 with the symmetry space group Pnma (COD-database: 1509782). After the laser irradiation, its XRD pattern matches with the Ag_2CrO_4 phase to the extent of 99.62%, and with the cubic Ag phase with symmetry space group Fm-3m (COD-database: 9012961) to the extent of 0.37%. Moreover, according to the Rietveld method, the Ag_2CrO_4 lattice parameters b and c have been slightly expanded, and the Rietveld-refined fractional coordinates display a minimal modification (the information extracted from the Rietveld method is displayed in Tables S.1-5 in the Supporting Information).

In the case of B, its diffraction pattern can be associated with the monoclinic crystal phase of α-Bi_2O_3 with the symmetry space group P21/c (COD-database: 9012546) to the extent of 96.75%, with the orthorhombic crystal phase of $Bi_2O_2CO_3$ with the symmetry space group Pna21 (COD-database: 1530018) to the extent of 2.19% and with the cubic crystal phase of δ-Bi_2O_3 with the

symmetry space group Pn-3m (COD-database: 1010311) to the extent of 1.04%. The impurities found in Bi_2O_3 respond to the fact that the pristine semiconductor was mechanically ground before the characterization. As previously reported by Streletskii A. and co-workers,[26] grinding in air can induce the formation of $Bi_2O_2CO_3$ due to the sorption of CO_2 from the air. The minimal presence of δ-Bi_2O_3 may come from the synthesis of Bi_2O_3 itself. After the laser irradiation, the most significant change is an increment in the $Bi_2O_2CO_3$ phase from 2.19% to 8.41% and a modification in its lattice parameters, which might be connected to the fact that the laser irradiation took place in the air, and as in the case of grinding, it is plausible that the semiconductor experiences sorption of CO_2 from the air, especially considering that in a laser ablation process, elements from the environment can interact with the plasma generated by the laser-matter interaction, allowing their incorporation in the ablated material.[27,28]

In the diffraction patterns that correspond to the mixtures 75A-25B, 50A-50B, and 25A-75B, it is possible to identify the previously described crystal phases of Ag_2CrO_4, α-Bi_2O_3, $Bi_2O_2CO_3$, and δ-Bi_2O_3, where their extent is closely related to the weight ratio between A and B, except for $Bi_2O_2CO_3$ (see Tables S.1-5 in the Supporting Information). In the particular case of the crystal phase $Bi_2O_2CO_3$, it seems to increment with the addition of Ag_2CrO_4, which might be a result of the size reduction of B as displayed in Fig. 2. If the size gets reduced, there is more surface that can undergo the sorption of CO_2.

Aside of the relation between the crystal phases and the weight ratio of the semiconductor mixtures, it is also possible to notice that regardless the A to B weight ratio, there is no any substantial change in the lattice parameters of the Ag_2CrO_4 and α-Bi_2O_3 crystal phases since the only changes fall within the standard deviation 10^{-3} Å. On the contrary, the lattice parameters of the δ-Bi_2O_3 and $Bi_2O_2CO_3$ crystal phases display various changes. On the one hand, the cell length a of the cubic δ-Bi_2O_3 slightly decreases as the amount of Ag_2CrO_4 increases, which, as suggested by Dilpuneet S. and co-workers[29] is related of the incorporation of oxygen atoms in the crystal structure, possibly from Ag_2CrO_4 or from sorbed CO_2. However, it is necessary to highlight that neither *Bi* nor *O* atoms display any change in the fractional coordinates that would

ratify the contraction of the crystal. Therefore, it is only possible to report that the amount of δ-Bi_2O_3 phase gets modified with the incorporation of Ag_2CrO_4. On the other hand, the lattice parameters of $Bi_2O_2CO_3$ do not change following any clear tendency. Nevertheless, when the amount of $Bi_2O_2CO_3$ in 25A-75B grows up to 9.13 wt%, the *a* and *b* lattice parameters get slightly expanded while the *c* parameter gets reduced, which is common when the crystal presents oxygen vacancies.[30]

After the laser irradiation, the presence of Ag_2CrO_4 and δ-Bi_2O_3 crystal phases got incremented, while the amount of α-Bi_2O_3 got decremented in all the cases. In parallel, the $Bi_2O_2CO_3$ crystal phase got incremented except for the mixture 50A-50B, where it does not only got decremented, but the Ag_2CrO_4 phase grown the most. Besides, the samples with the largest amount of Ag_2CrO_4, i.e., 75A-25B (F) and 50A-50B (F), also display the presence of the cubic Ag phase. The changes can be connected to the size reduction of the semiconductors and the segregation of metallic NPs. On the one hand, as previously noticed, the size reduction of B seems to favor the presence of the δ-Bi_2O_3 and $Bi_2O_2CO_3$ phases and reduces the one of α-Bi_2O_3. On the other hand, as described above, the femtosecond laser irradiation leads to the formation of Ag NPs, however, it is not possible to infer from the XRD patterns the existence of the Bi NPs since the most intense peaks of the metallic Bi phase match with those belonging to the α-Bi_2O_3 one. Moreover, since the laser irradiation does not lead to any mechanism that could allow the formation of more Ag_2CrO_4, the increment in this crystal phase could be related to the fact that the α-Bi_2O_3 one, which has more intense peaks gets reduced, allowing a better fitting of the Ag_2CrO_4 phase.

Finally, the lattice parameters of most of the crystal phases did not experience any significant change after the laser irradiation, except for $Bi_2O_2CO_3$ that change when in 25A-75B the crystal phase grows up to 17.69 wt%. As described above, the modifications can be related to the fact that the ablation process may induce oxygen vacancies, which are in general ratified by the modifications of the fractional coordinates, where those corresponding to the *Bi* atoms switch to smaller values, those belonging to the *C* atoms switch to larger values, and those belonging to the *O* atoms change without a clear tendency.

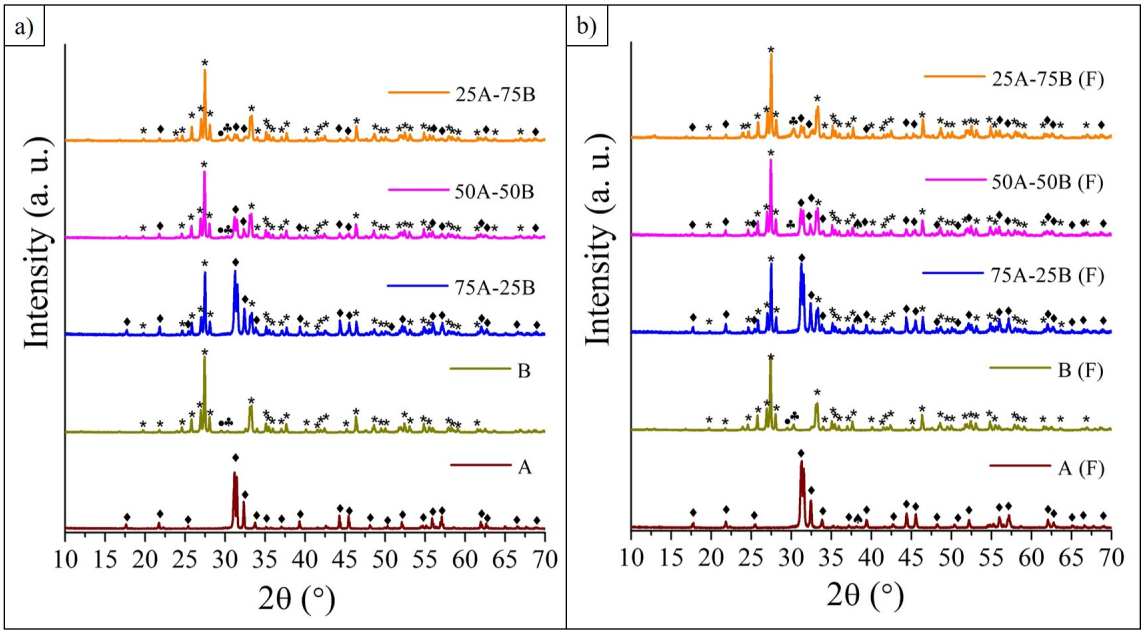

Figure 3: XRD spectra for different samples, a) before and b) after being subject to femtosecond laser irradiation. The symbol ◆ represents the Ag_2CrO_4 phase, ∗ the α-Bi_2O_3 phase, • the δ-Bi_2O_3 phase, ♣ the $Bi_2O_2CO_3$ phase, and ♠ Ag phase.

The HR-TEM micrographs (Fig. 4) taken at the border sides of the irradiated heterostructures confirm the creation of NPs and the coexistence of the above described crystalline phases. Particularly, in the irradiated sample 75A-25B it is possible to identify in the zone Ⓐ, which has many NPs, the interplanar distances (2.384 ± 0.098) Å, (2.044 ± 0.021) Å, (3.127 ± 0.022) Å and (2.298 ± 0.019) Å that can be associated to the Miller indices (111), (200) of Ag (COD-database: 9012961), and (012), (110) of Bi (COD-database: 2310889) phases, respectively. In the zone Ⓑ, where no NPs are found, it is possible to identify the interplanar distances (6.700 ± 0.033) Å, (2.918 ± 0.016) Å, (2.847 ± 0.098) Å, and (2.531 ± 0.082) Å, which correspond to the indices (040), (161) of $Bi_2O_2CO_3$ (COD-database: 1530018), and (121), (221) of Ag_2CrO_4 (COD-database: 1509782) phases, respectively.

For the irradiated 50A-50B, the zone Ⓒ that is filled with NPs allows to observe the interplanar distances (2.216 ± 0.080) Å, (1.195 ± 0.060) Å, (1.246 ± 0.030) Å, and (2.022 ± 0.013) Å that correspond to the Miller indices (110), (208) of Bi (COD-database: 2310889), and (311), (200) of Ag (COD-database: 9012961) phases, respectively. The zone Ⓓ, which represents the places

where there are NPs over the heterostructure's surface, it is possible to identify the interplanar distances (1.363 ± 0.017) Å, (1.556 ± 0.010) Å, and (3.737 ± 0.012) Å that can be associated to the indices (314), and (-312) of α-Bi_2O_3 (COD-database: 9012546), and (121) of $Bi_2O_2CO_3$ (COD-database: 1530018) phases, respectively.

In the case of the irradiated 25A-75B, the zone Ⓔ, where the disposition is the same as the previous one, exhibits the interplanar distances (1.007 ± 0.008) Å, (1.305 ± 0.008) Å, (1.304 ± 0.013) Å, and (1.359 ± 0.060) Å, which can be ascribed to the indices (015) of Ag_2CrO_4 (COD-database: 1509782), and (-233), (-233) and (015) of α-Bi_2O_3 (COD-database: 9012546) phases, respectively. The zone Ⓕ, which represents a zone where the NPs and the heterostructure are clearly separated, enables the measurement of the interplanar distances (2.214 ± 0.016) Å, (2.977 ± 0.020) Å, (2.846 ± 0.033) Å, and (2.080 ± 0.019) Å that can be associated to the indices (152), (161) of $Bi_2O_2CO_3$ (COD-database: 1530018) and (120), (211) of Bi (COD-database: 2310889) phases, respectively.

Finally, complementary EDX Mapping images displayed in Fig. S1-3 in the Supporting Information exhibit that regardless of each semiconductor's ratio, the laser radiation leads to a homogeneous elemental distribution. Moreover, the corresponding EDS spectra also show the atomic percentage of the samples even-up after laser irradiation. This indicates that the laser treatment enables the production of tight heterojunctions.

Raman Spectroscopy

Fig.5 displays the comparison between the samples before and after the laser irradiation. Where in general, it is possible to identify substantial changes after the mixing of the samples and irradiation.

In the case of sample A, which as ratified by XRD is composed purely by Ag_2CrO_4 with the symmetry space group, Pnma has 36 Raman-active modes: $11A_g + 7B_{1g} + 11B_{2g} + 7B_{3g}$, where 18 are internal modes, and the other 18 are external rotational and translational modes of the CrO_4 group. The Raman peaks located in the 750–900 cm^{-1} region correspond to the stretching modes, the peaks located in the 350–450 cm^{-1} region to the bending modes, and those located below 150

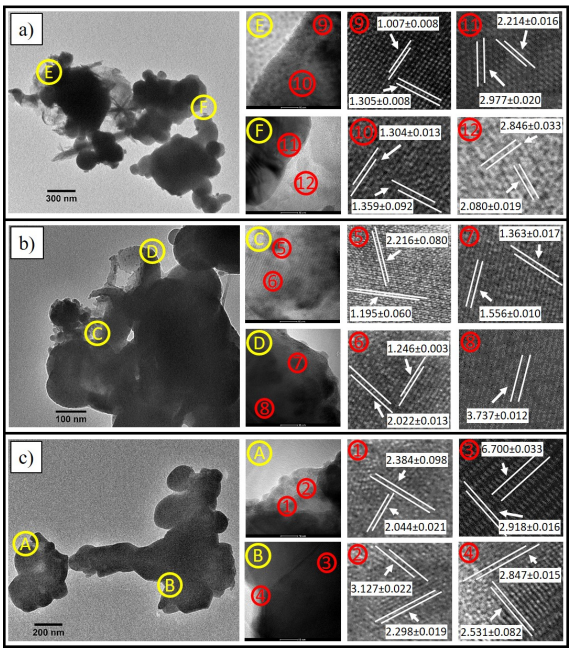

Figure 4: TEM and HR-TEM micrographs of a) 25A-75B, b) 50A-50B, and c) 75A-25B after being subject to the laser irradiation. The distances indicated in the HR-TEM images are in (Å) units.

cm^{-1} correspond to the rotational and translational modes.[31] As it is displayed in Fig.5 a), the pristine A clearly shows the peaks related to the bending and stretching modes, but those related to the rotational and translational modes are harder to observe, which is something common while measuring Ag_2CrO_4 at ambient conditions. The irradiated sample (A (F)) shows broadened peaks belonging to the bending and stretching modes, a more intense peak belonging to the rotational and translational modes, and a new peak in the 530-615 cm^{-1} region (indicated by an asterisk symbol in the graph). The changes related to the peak broadening and the increment in the intensity of the peak below 150 cm^{-1} can be attributed to a combination of the semiconductor size reduction, as observed in Fig. 2, and an increment in the short- and long-range disorder.[32] As discussed above, the laser ablation of Ag_2CrO_4 not only leads to the material's size reduction, but also to the segregation of heavy elements to form metal NPs. This process may induce short- and long-range disorder in the crystal. An alternative explanation for the disorder increment relies on the interaction with the ablation plasma. As previously reported, when Ag_2CrO_4 is subject to high pressure, it undergoes a phase transition, which is reversible when reducing the pressure values.[31]

As the plasma has a lifetime in the temporal region of $\sim 10^{-9}$ s, it is possible to infer that the material that was exposed to the plasma (see Fig. 1 for reference) could undergo a rapid phase transition followed by the reverse phase transition after the plasma extinguished, leading in this way to the increment of disorder in the crystal.

Besides, the new peak found in the 530-615 cm^{-1} region can be identified as a Raman-active stretching mode A_{1g} of the Cr-O bond commonly found in the chromium oxide Cr_2O_3 group.[33] This is not a mode found in the Ag_2CrO_4 semiconductor because it is composed only by AgO_6, AgO_4, and CrO_4 atomic clusters, but the laser modification used in the current work can enable the recombination of the constituent elements of the semiconductor due to the interaction with the plasma plume, leading to the formation of Cr_2O_3.

In the case of sample B, even when the specimen is composed by a mixture of α-Bi_2O_3 with the symmetry space group P21/c, δ-Bi_2O_3 Pn-3m, and $Bi_2O_2CO_3$ Pna21, it is possible to clearly identify only 11 out of the 30 Raman-active modes of α-Bi_2O_3, $15A_g$ + $15B_g$, which is typical when the Raman spectrum of α-Bi_2O_3 plus additional bismuth oxides derivatives is taken at room temperature.[34,35] The identified modes located below 120 cm^{-1} belong to the vibration of Bi atoms (Bi-Bi), the ones found in the 120-150 cm^{-1} region belong to the vibrations of the *Bi* and *O* atoms (Bi-O), and those above 150 cm^{-1} belong to the vibrations of the *O* atoms (O-O).[36] The irradiated sample (B (F)) shows the same peaks but broadened, giving the impression that the near peaks combine. As the semiconductor undergoes laser irradiation with the same parameters used to irradiate A, it is expected to get a similar Raman spectrum modification due to the same reasons. Moreover, the size reduction displayed in the SEM micrographs supports this assumption.

For the different semiconductor mixtures, the Raman spectra displayed in Fig.5 c) seem to be a combination of the separate Ag_2CrO_4 and Bi_2O_3 phases, except for 75A-25B and 25A-75B, which display a new Raman-mode centered at the wavenumbers 580 and 522 cm^{-1}, respectively (indicated by a capital delta symbol and a capital phi symbol, respectively). Both modes are neither typical for Ag_2CrO_4 nor for Bi_2O_3, but they are typical for the Cr-O bond from Cr_2O_3,[33] and O-O bond from α-Bi_2O_3 after increasing its oxygen defects by annealing in air.[37] As the mechanical

grind treatment was used to get a uniform mixture between the semiconductors, it is possible to infer that during the treatment, the semiconductors underwent a partial destruction of their crystal structure due to the accumulation of defects, as suggested in 1996 by Fukunaga et al. for the case of trigonal Se.[38] Therefore, the occurrence of both Raman-modes can be related to the crystalline modification of the corresponding mixtures. In the case of 75A-25B, the amount of Ag_2CrO_4 is larger and therefore it is expected to get a larger amount of by-products coming from the semiconductor, which can decompose into Ag, O_2 and Cr_2O_3.[39] For 25A-75B, the oxygen defects get incremented in Bi_2O_3, which is evident by the appearance of the mode located at 522 cm^{-1}, which outshines the contribution of the modes belonging to the Ag_2CrO_4 by-products because they are in a lower amount.

After the laser treatment, all the mixtures display similar Raman spectra with 5 peaks located in the regions 80-210, 300-400, 470-600, and two peaks at 700-900 cm^{-1} (indicated by arrows in Fig.5 c)), which seem to be a combination of the broad Raman peaks displayed by A (F) and B (F), except for the case of the modes belonging to (O-O) from α-Bi_2O_3, which seem to disappear after the laser treatment, and an increment in the peak centered at 522 cm^{-1}, which as discussed above can be related to an increase of oxygen vacancy defects in α-Bi_2O_3. Besides, there is not a large difference between the spectra of the irradiated samples, a closer inspection only reveals a tendency of increasing intensity for the peak centered at 522 cm^{-1} as the amount of B increases in the mixture, and a merge of the two peaks that correspond to the stretching modes of Ag_2CrO_4 as the amount of A is reduced.

The Raman spectra, therefore, ratifies that the laser irradiation provides oxygen vacancies to all the heterostructures, where the largest amount of them can be found in mixtures containing a larger amount of B. Besides, the irradiation process caused structural changes as a disorder increment in the constituent crystals, which can be interpreted as a more intimate junction of A and B while using the laser radiation.

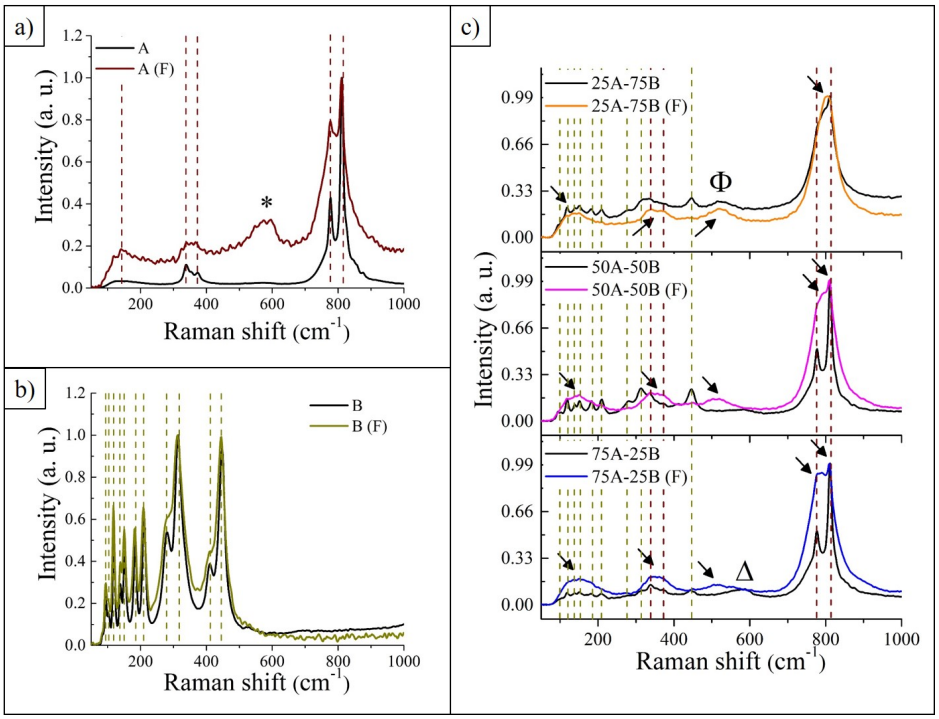

Figure 5: FT-Raman spectra of the samples before and after (F) being subject to the laser irradiation, a) A, b) B, and c) mixtures.

UV–Vis DRS

The diffusive spectra of the different samples (Fig. 6 a)) show information that substantially agrees with the XRD, HR-TEM, and Raman spectroscopy results. On the one hand, the pristine sample A has a reflectance spectrum that matches those previously reported elsewhere,[21] and the pristine sample B displays a reflectance spectrum that corresponds to a combination of the crystalline phases α-Bi_2O_3 and $Bi_2O_2CO_3$.[40,41] On the other hand, the mixtures seem to be a combination of the spectra that belong to the pristine A and B; they show double reflectance edges that do not entirely match with those of pristine A and B, there is a shift to shorter wavelengths for the edges that resemble the one of A, and a shift to longer wavelengths for those that resemble the one of B. The corresponding shifts can be attributed to the electron-hole transition between the composing semiconductors. Besides, since these semiconductors are characterized by absorption spectra governed mainly by indirect allowed electronic transitions, the optical band gap (E_g) was extracted from the Kubelka-Munk equation $\alpha h\nu = C(h\nu - E_g)^2$, where α represents the absorption

coefficient, hν the photon energy, and C a proportionality constant.[42]

The calculations show that the E_g of the pristine A has a similar value as the one conventionally obtained for Ag_2CrO_4 when it is synthesized by the co-precipitation method,[42] the pristine B shows an E_g value that corresponds to a combination of the one for α-Bi_2O_3 and $Bi_2O_2CO_3$, 2.80 and 3.42 eV, respectively,[43,44] and in the case of the mixtures, no E_g entirely match those values belonging to the pristine A or B, which indicates that the grinding process effectively allows the formation of heterojunctions between the composing semiconductors.

After the laser irradiation, the diffusive spectra of all the samples display significant changes (Fig. 6 b)). In the case of B, the reflectance gets incremented for longer wavelengths, which responds to the increment of the $Bi_2O_2CO_3$ phase, there are no significant changes in the case of A, and in all the mixtures the edge that corresponds to the B sample gets highly reduced in intensity being finally hidden by the reflectance behavior that resembles the one of the A sample. Moreover, the edge that corresponds to A fairly concurs at the same wavelength for all the mixtures. The E_g values also show essential changes; after the laser irradiation, the optical band gap of B gets wider, which coincides with the increment in the $Bi_2O_2CO_3$ phase observed in its XRD pattern. The E_g value of A gets incremented from 1.84 to 1.94 eV, which, as reported elsewhere, corresponds to the semiconductor's size decrement.[21] Finally, the clearly observable double E_g values exhibited by the non-laser-treated mixtures change to a combination of an accentuated E_g value that is close to the one of A after being subject to the laser irradiation, and a difficult to observe straight segment in the Kubelka-Munk plot that should correspond to the reflectance edge contribution of B. The vanishing of the E_g value that resembles the one of the B sample can occur due to the disorder increment in the B's crystal network. As interpreted from the Raman spectra, the laser radiation provides defects to the heterostructure's constituent crystals. However, the lower definition of the modes that correspond to α-Bi_2O_3 suggests that this is the crystal that gets more affected by the inclusion of the defects, and consequently its contribution to the reflectance spectra gets diminished leading to the hiding of the E_g value that corresponds to B by the one of A. This results indicate that the addition of Ag_2CrO_4 to a crystal with wide band gap like α-Bi_2O_3 expands the optical

response of the heterostructure to a wider spectral range of the solar radiation.

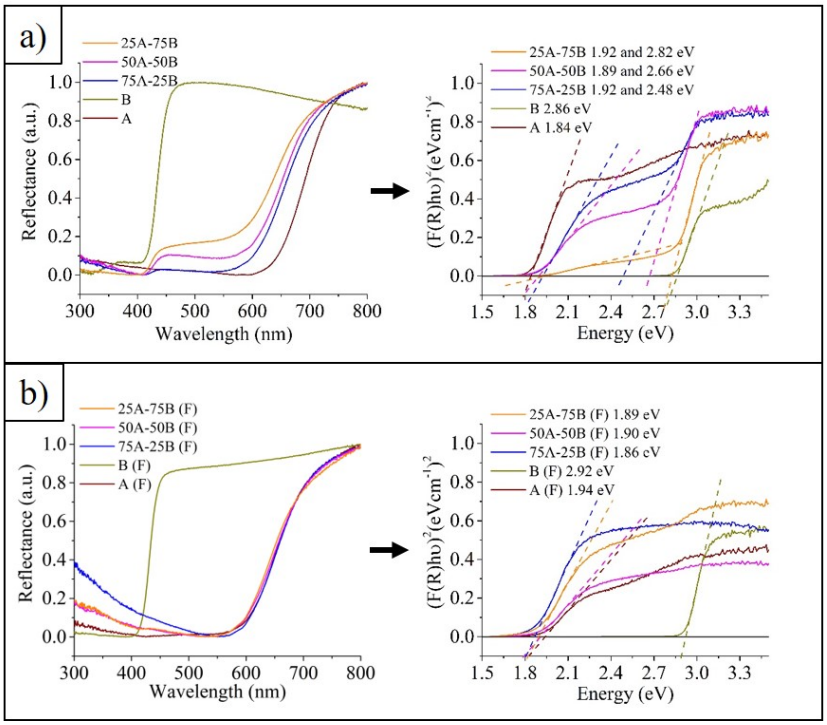

Figure 6: UV-Vis DRS spectra (left-side) and calculated band gap (right-side) of a) the samples before and b) after being subject to the laser irradiation.

Photoluminescence

The PL spectra displayed in Fig. 7 provide a more accurate picture of the defects increment implications after the laser irradiation. In the case of A, it is possible to observe two peaks, one centered at 461 nm and another at 760 nm. In general, both peaks come from multiphonon and multilevel processes within the material's bandgap. The more energetic peak corresponds to the recombination of electron holes due to the disorder degree in the composing clusters of Ag_2CrO_4, and the one centered at the longer wavelengths to its oxygen vacancies[42] (the scheme for the photoluminescence mechanism is displayed in Fig. S4 a) in the Supporting Information). As it is observed in Fig. 7 a), the laser irradiation reduces the relative intensities of bands around 760 nm and 461 nm, which were associated with oxygen vacancies and disorder, respectively. Therefore, the laser irradiation reduces the density of oxygen vacancies in the semiconductor and favors the increase

of the crystal clusters' disorder, which is in agreement with the observed changes of XRD, which were associated with the formation of Ag NPs. In the case of B, the PL spectra of the samples before and after laser irradiation are formed by a broadband emission in the wavelength region 400-850 nm, which is usually associated to the Bi ions in α-Bi_2O_3; the emission at longer wavelengths corresponds to the electronic transition $^2P_{3/2} \rightarrow {}^2P_{1/2}$ of Bi^{2+}, and the emission at shorter wavelengths to the $^3P_1 \rightarrow {}^1S_0$ transition of Bi^{3+}. The intensity of the emission is usually attributed to defects or impurities in the crystal, emission shoulders at short wavelengths to quantum size effects, and shoulders at long wavelengths to the presence of oxygen vacancies[45] (see Fig. S4 b) in the Supporting Information). In the case of non-irradiated B, the most intense peak is centered at 612 nm and has two shoulders, one at 514 nm and the other at 762 nm, which confirms the presence of defects in the α-Bi_2O_3 crystal. Similarly, the emission spectrum after the laser irradiation shows an intense peak centered at 616 nm and two shoulders, one at 468 nm and the other at 790 nm. At first sight, the higher intensity of the non-irradiated B may suggest that in contrast to the previous results, it has a larger amount of defects than the irradiated sample. However, the decrease in intensity could be due to wavelength shift of the shoulders, which in turn implies the presence of α-Bi_2O_3 and Bi NPs with sizes < 10 nm that would be susceptible to quantum size effects,[46] and a larger amount of oxygen vacancies.

In the case of the mixtures, the PL emission spectra seem to be the combination of those belonging to A and B. The non-irradiated samples show a decreasing emission in the wavelength region 550-700 nm (Fig. 7 c) grey frame), and a shift of the peak enclosed in the region 350-550 nm (Fig. 7 c) green frame) to longer wavelengths as the amount of B (i.e. Bi_2O_3) decreases, which can be due to the reduction of the emission coming from the electronic transitions of the Bi ions. Besides, the overall emission intensity does not show any specific tendency regarding the ratio of the composing crystals, but the one for 50A-50B is the lowest one. Since a small intensity in the PL spectra is related to the suppression in the recombination of photoinduced charge carriers,[47] the PL results indicate that the production of the heterostructure 50A-50B can be of particular interest for its potential use in applications requiring an efficient transformation of sunlight into charge

carriers.

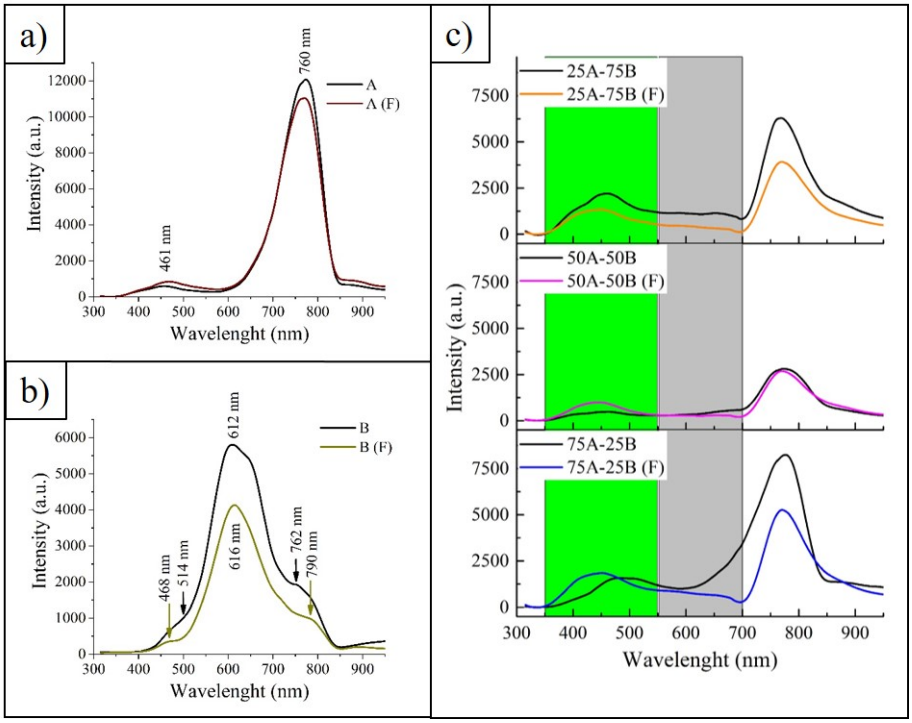

Figure 7: PL spectra of the samples before and after (F) irradiation a) A, b) B, and c) mixtures.

After the laser irradiation, the PL spectra of all the samples get the same shape. However, they show the same intensity variations observed in the non-irradiated samples, the highest for the sample with the largest amount of A, and the lowest for the sample 50A-50B. As interpreted from the Raman spectroscopy and UV-Vis DRS results, the laser-induced disorder increment in the α-Bi_2O_3 crystal may enable a more significant contribution of PL emission. Moreover, the laser irradiation also changes the relative intensity of the stronger PL bands. In particular, the laser irradiation decreases the relative intensity of the bands around 800nm and 450nm, which confirms an increasing contribution of emission due to the α-Bi_2O_3 crystal. Consequently, in contrast with the non-irradiated samples, after the laser irradiation, it is possible to observe an equal contribution to the corresponding PL emission in the wavelength region 550-700 nm that corresponds to α-Bi_2O_3. Besides, it is also essential to notice that in comparison with the non-irradiated samples, the irradiated once display an overall lower PL emission intensity.

Therefore, the use of laser irradiation improves the heterojunctions interactions benefiting the

suppression in the recombination of photogenerated carriers, a behaviour that is expected to enhance the applicability of the corresponding materials towards applications activated by photonic sources.

Conclusions

The current study serves to shed light on the impact behind the use of femtosecond laser radiation to generate heterojunctions. In particular, the composing elements of the produced heterostructures were Ag_2CrO_4 and α-Bi_2O_3, two photosensitive semiconductors that are known to be precursors for the laser-mediated segregation of NPs.

As expected, the laser irradiation of the pristine semiconductors leads to the segregation of the NPs, but also increment in crystalline disorder for Ag_2CrO_4, an increment of oxygen vacancies for α-Bi_2O_3, an increment of crystal impurities, size reduction, and suppression in the recombination of photoinduced charge carriers. In the case of the different semiconductor mixtures, the simple mechanical grinding enables a basic junction between the semiconductors that, among the most relevant features, permits the coexistence of two different band gaps. This fact ultimately means there are two kinds of charge carriers with different energies, which separation and spread through the heterostructure could be exploited in, for instance, multiple catalytic processes. The laser radiation treatment in the counterpart enables a more intimate junction where a single narrow band gap value reminds, and the recombination of the photoinduced charge carriers gets reduced at any ratio of composing elements. Besides, since the 50 to 50 wt% semiconductor's mixture displays the lowest amount of impurities and the most reduced PL emission before and after the laser treatment, this material could be of particular interest in applications where the transformation of the sunlight radiation into charge carriers is required, such as photocatalysis or photovoltaic cell manufacturing.

In summary, heterojunctions between Ag_2CrO_4 and Bi_2O_3 with reduced recombination of charge carriers have been successfully obtained by their in-situ femtosecond laser irradiation. As revealed in the current manuscript, this is a promising treatment towards developing tight het-

erojunctions with improved optical capabilities, which may find a niche of exploitation in light-powered environmental remediation and energy-related applications. Moreover, using a laser as a working tool, which is spatially confined, permits envisaging future strategies to form highly localized heterojunctions, permitting their tailored design.

Acknowledgement

The authors would like to acknowledge the economic support from the Ministry of Education, Youth and Sports in the Czech Republic under the program Research Infrastructures NanoEnviCz (Project No. LM2018124), program International Mobilities of Researchers at the TUL (Project No. CZ.02.2.69/0.0/0.0/16_027/0008493), European Structural and Investment Funds in the framework of the Operational Programme Research, Development and Education – project entitled Hybrid Materials for Hierarchical Structures (HyHi, Reg. No. CZ.02.1.01/0.0/0.0/16/_019/0000843), National Council for Scientific and Technological Development – CNPq, Coordenação de Aperfeiçoamento de Pessoal de Nível Superior-Brasil (CAPES) - Finance Code 001, FAPESP-CDMF (2013/07296-2), Generalitat Valenciana (PROMETEO/2020/029), Ministerio de Ciencia e Innovación (PID2019-110927RB-I00), the Ministerio de Ciencia, Innovación y Universidades (Spain) projects PGC2018-094417-B-I00, MAT2016-80410-P, and Universitat Jaume I for the projects UJI-B2019-30 and UJI-B2019-41. We also thank the Servei Central d'Instrumentació Científica (SCIC) of the University Jaume I for the use of the femtosecond laser. Finally, the authors would also like to acknowledge Marcelo Assis for the preparation of the Ag_2CrO_4 powder.

References

(1) Lu, L.; Zheng, T.; Wu, Q.; Schneider, A. M.; Zhao, D.; Yu, L. Recent advances in bulk heterojunction polymer solar cells. *Chemical reviews* **2015**, *115*, 12666–12731.

(2) Melianas, A.; Kemerink, M. Photogenerated Charge Transport in Organic Electronic Materials: Experiments Confirmed by Simulations. *Advanced Materials* **2019**, *31*, 1806004.

(3) Xu, C.; Anusuyadevi, P. R.; Aymonier, C.; Luque, R.; Marre, S. Nanostructured materials for photocatalysis. *Chemical Society Reviews* **2019**, *48*, 3868–3902.

(4) Torres-Mendieta, R.; Mondragón, R.; Puerto-Belda, V.; Mendoza-Yero, O.; Lancis, J.; Juliá, J. E.; Mínguez-Vega, G. Characterization of tin/ethylene glycol solar nanofluids synthesized by femtosecond laser radiation. *ChemPhysChem* **2017**, *18*, 1055–1060.

(5) Sahoo, D. P.; Nayak, S.; Reddy, K. H.; Martha, S.; Parida, K. Fabrication of a $Co(OH)_2$/ZnCr LDH "p–n" heterojunction photocatalyst with enhanced separation of charge carriers for efficient visible-light-driven H_2 and O_2 evolution. *Inorganic chemistry* **2018**, *57*, 3840–3854.

(6) Yuan, N.; Zhang, J.; Zhang, S.; Chen, G.; Meng, S.; Fan, Y.; Zheng, X.; Chen, S. What Is the Transfer Mechanism of Photoexcited Charge Carriers for g-C_3N_4/TiO_2 Heterojunction Photocatalysts? Verification of the Relative p–n Junction Theory. *The Journal of Physical Chemistry C* **2020**, *124*, 8561–8575.

(7) Yonezawa, T.; Čempel, D.; Nguyen, M. T. Microwave-induced plasma-in-liquid process for nanoparticle production. *Bulletin of the Chemical Society of Japan* **2018**, *91*, 1781–1798.

(8) Kanitz, A.; Kalus, M.; Gurevich, E.; Ostendorf, A.; Barcikowski, S.; Amans, D. Review on experimental and theoretical investigations of the early stage, femtoseconds to microseconds processes during laser ablation in liquid-phase for the synthesis of colloidal nanoparticles. *Plasma Sources Science and Technology* **2019**, *28*, 103001.

(9) Vorobyev, A. Y.; Guo, C. Direct femtosecond laser surface nano/microstructuring and its applications. *Laser & Photonics Reviews* **2013**, *7*, 385–407.

(10) Jiang, L.; Wang, A.-D.; Li, B.; Cui, T.-H.; Lu, Y.-F. Electrons dynamics control by shap-

ing femtosecond laser pulses in micro/nanofabrication: modeling, method, measurement and application. *Light: Science & Applications* **2018**, *7*, 17134–17134.

(11) Chichkov, B. N.; Momma, C.; Nolte, S.; Von Alvensleben, F.; Tünnermann, A. Femtosecond, picosecond and nanosecond laser ablation of solids. *Applied physics A* **1996**, *63*, 109–115.

(12) Assis, M.; Cordoncillo, E.; Torres-Mendieta, R.; Beltrán-Mir, H.; Mínguez-Vega, G.; Oliveira, R.; Leite, E. R.; Foggi, C. C.; Vergani, C. E.; Longo, E., et al. Towards the scale-up of the formation of nanoparticles on α-Ag_2WO_4 with bactericidal properties by femtosecond laser irradiation. *Scientific reports* **2018**, *8*, 1–11.

(13) Assis, M.; Macedo, N. G.; Machado, T. R.; Ferrer, M. M.; Gouveia, A. F.; Cordoncillo, E.; Torres-Mendieta, R.; Beltrán-Mir, H.; Mínguez-Vega, G.; Leite, E. R., et al. Laser/electron irradiation on indium phosphide (InP) semiconductor: Promising pathways to in situ formation of indium nanoparticles. *Particle & Particle Systems Characterization* **2018**, *35*, 1800237.

(14) Assis, M.; Cordoncillo, E.; Torres-Mendieta, R.; Beltrán-Mir, H.; Mínguez-Vega, G.; Gouveia, A. F.; Leite, E.; Andrés, J.; Longo, E. Laser-induced formation of bismuth nanoparticles. *Physical Chemistry Chemical Physics* **2018**, *20*, 13693–13696.

(15) Machado, T. R.; Macedo, N. G.; Assis, M.; Donate-Buendia, C.; Mínguez-Vega, G.; Teixeira, M. M.; Foggi, C. C.; Vergani, C. E.; Beltrán-Mir, H.; Andres, J., et al. From complex inorganic oxides to Ag–Bi nanoalloy: Synthesis by femtosecond laser irradiation. *ACS omega* **2018**, *3*, 9880–9887.

(16) dos Santos, C. C.; de Assis, M.; Machado, T. R.; dos Santos Pereira, P. F.; Minguez-Vega, G.; Cordoncillo, E.; Beltran-Mir, H.; Doñate-Buendía, C.; Andrés, J.; Longo, E. Proof-of-Concept Studies Directed toward the Formation of Metallic Ag Nanostructures from Ag_3PO_4 Induced by Electron Beam and Femtosecond Laser. *Particle & Particle Systems Characterization* **2019**, *36*, 1800533.

(17) Assis, M. d.; Robeldo, T.; Foggi, C. C.; Kubo, A.; Mínguez-Vega, G.; Condoncillo, E.; Beltran-Mir, H.; Torres-Mendieta, R.; Andrés, J.; Oliva, M., et al. Ag Nanoparticles/α-Ag_2WO_4 Composite Formed by Electron Beam and Femtosecond Irradiation as Potent Antifungal and Antitumor Agents. *Scientific Reports* **2019**, *9*, 1–15.

(18) Lemos, P.; Silva, G.; Roca, R. A.; Assis, M. d.; Torres-Mendieta, R.; Beltrán-Mir, H.; Mínguez-Vega, G.; Cordoncillo, E.; Andrés, J.; Longo, E. Laser and electron beam-induced formation of Ag/Cr structures on Ag_2CrO_4. *Physical Chemistry Chemical Physics* **2019**, *21*, 6101–6111.

(19) Macedo, N. G.; Machado, T. R.; Roca, R. A.; Assis, M.; Foggi, C. C.; Puerto-Belda, V.; Mínguez-Vega, G.; Rodrigues, A.; San-Miguel, M. A.; Cordoncillo, E., et al. Tailoring the bactericidal activity of Ag nanoparticles/α-Ag_2WO_4 composite induced by electron beam and femtosecond laser irradiation: integration of experiment and computational modeling. *ACS Applied Bio Materials* **2019**, *2*, 824–837.

(20) Askari, P.; Mohebbi, S.; Do, T.-O. High performance plasmonic activation of Ag on β-Ag_2WO_4/$BiVO_4$ as nanophotocatalyst for oxidation of alcohols by incident visible light. *Journal of Photochemistry and Photobiology A: Chemistry* **2018**, *367*, 56–65.

(21) Xu, D.; Cao, S.; Zhang, J.; Cheng, B.; Yu, J. Effects of the preparation method on the structure and the visible-light photocatalytic activity of Ag_2CrO_4. *Beilstein journal of nanotechnology* **2014**, *5*, 658–666.

(22) Lutterotti, L.; Bortolotti, M.; Ischia, G.; Lonardelli, I.; Wenk, H. Rietveld texture analysis from diffraction images. *Z. Kristallogr. Suppl* **2007**, *26*, 125–130.

(23) Escobedo-Morales, A.; Ruiz-López, I.; Ruiz-Peralta, M. d.; Tepech-Carrillo, L.; Sánchez-Cantú, M.; Moreno-Orea, J. Automated method for the determination of the band gap energy of pure and mixed powder samples using diffuse reflectance spectroscopy. *Heliyon* **2019**, *5*, e01505.

(24) Ding, K.; Ye, L. *Laser shock peening: performance and process simulation*; Woodhead Publishing, 2006.

(25) Assis, M.; Carvalho de Oliveira, M.; Machado, T. R.; Macedo, N. G.; Costa, J. P. C.; Gracia, L.; Andrés, J.; Longo, E. In Situ Growth of Bi Nanoparticles on $NaBiO_3$, δ-, and β-Bi_2O_3 Surfaces: Electron Irradiation and Theoretical Insights. *The Journal of Physical Chemistry C* **2019**, *123*, 5023–5030.

(26) Streletskii, A.; Kolbanev, I.; Vorob'eva, G.; Leonov, A.; Borunova, A.; Dubinskii, A. Mechanochemistry of Bi_2O_3. 1. Defect Structure and Reactivity of Mechanically Activated Bi_2O_3. *Colloid Journal* **2019**, *81*, 567–574.

(27) Baba, M.; Jia, T.; Suzuki, M.; Kuroda, H. Femtosecond laser induced nanowire technique and its applications. *ISRN Nanotechnology* **2011**, *2011*.

(28) Andreeva, Y.; Sharma, N.; Rudenko, A.; Mikhailova, J.; Sergeev, M.; Veiko, V. P.; Vocanson, F.; Lefkir, Y.; Destouches, N.; Itina, T. E. Insights into Ultrashort Laser-Driven Au: TiO_2 Nanocomposite Formation. *The Journal of Physical Chemistry C* **2020**, *124*, 10209–10219.

(29) Aidhy, D. S.; Nino, J. C.; Sinnott, S. B.; Wachsman, E. D.; Phillpot, S. R. Vacancy-Ordered Structure of Cubic Bismuth Oxide from Simulation and Crystallographic Analysis. *Journal of the American Ceramic Society* **2008**, *91*, 2349–2356.

(30) Lu, Y.; Huang, Y.; Zhang, Y.; Cao, J.-j.; Li, H.; Bian, C.; Lee, S. C. Oxygen vacancy engineering of Bi_2O_3/$Bi_2O_2CO_3$ heterojunctions: implications of the interfacial charge transfer, NO adsorption and removal. *Applied Catalysis B: Environmental* **2018**, *231*, 357–367.

(31) Santamaría-Pérez, D.; Bandiello, E.; Errandonea, D.; Ruiz-Fuertes, J.; Gomis, O.; Sans, J. A.; Manjón, F. J.; Rodríguez-Hernández, P.; Munoz, A. Phase behavior of Ag_2CrO_4 under compression: structural, vibrational, and optical properties. *The Journal of Physical Chemistry C* **2013**, *117*, 12239–12248.

(32) Gouadec, G.; Colomban, P. Raman Spectroscopy of nanomaterials: How spectra relate to disorder, particle size and mechanical properties. *Progress in crystal growth and characterization of materials* **2007**, *53*, 1–56.

(33) Brown, D.; Cunningham, D.; Glass, W. The infrared and Raman spectra of chromium (III) oxide. *Spectrochimica Acta Part A: Molecular Spectroscopy* **1968**, *24*, 965–968.

(34) Betsch, R. J.; White, W. B. Vibrational spectra of bismuth oxide and the sillenite-structure bismuth oxide derivatives. *Spectrochimica Acta Part A: Molecular Spectroscopy* **1978**, *34*, 505–514.

(35) Nuñez-Briones, A.; García-Cerda, L.; Rodríguez-Hernández, J.; Aguilar-González, M.; Puente-Urbina, B.; Mendoza-Mendoza, E. Synthesis, structural characterization, and photocatalytic activity of Bi-based nanoparticles. *International Journal of Applied Ceramic Technology* **2018**, *15*, 101–110.

(36) Denisov, V.; Ivlev, A.; Lipin, A.; Mavrin, B.; Orlov, V. Raman spectra and lattice dynamics of single-crystal. *Journal of Physics: Condensed Matter* **1997**, *9*, 4967.

(37) Vila, M.; Díaz-Guerra, C.; Piqueras, J. Luminescence and Raman study of α-Bi_2O_3 ceramics. *Materials Chemistry and Physics* **2012**, *133*, 559–564.

(38) Fukunaga, T.; Utsumi, M.; Akatsuka, H.; Misawa, M.; Mizutani, U. Structure of amorphous Se prepared by milling. *Journal of non-crystalline solids* **1996**, *205*, 531–535.

(39) Wu, Y.-P.; Chiang, H.-Y.; Hsiang, H.-I. $AgCrO_2$ formation mechanism during silver inner electrode and Fe–Si–Cr alloy powder co-firing in metal multilayer chip power inductors. *Journal of Materials Science: Materials in Electronics* **2019**, *30*, 8080–8088.

(40) Iyyapushpam, S.; Nishanthi, S.; Padiyan, D. P. Synthesis of β-Bi_2O_3 towards the application of photocatalytic degradation of methyl orange and its instability. *Journal of Physics and Chemistry of Solids* **2015**, *81*, 74–78.

(41) Leontie, L.; Caraman, M.; Alexe, M.; Harnagea, C. Structural and optical characteristics of bismuth oxide thin films. *Surface Science* **2002**, *507*, 480–485.

(42) Silva, G. S.; Gracia, L.; Fabbro, M. T.; Serejo dos Santos, L. P.; Beltrán-Mir, H.; Cordoncillo, E.; Longo, E.; Andrés, J. Theoretical and experimental insight on Ag_2CrO_4 microcrystals: synthesis, characterization, and photoluminescence properties. *Inorganic chemistry* **2016**, *55*, 8961–8970.

(43) Han, A.; Sun, J.; Chuah, G. K.; Jaenicke, S. Enhanced p-cresol photodegradation over BiOBr/Bi_2O_3 in the presence of rhodamine B. *RSC advances* **2016**, *7*, 145–152.

(44) Huang, H.; Tian, N.; Jin, S.; Zhang, Y.; Wang, S. Syntheses, characterization and nonlinear optical properties of a bismuth subcarbonate $Bi_2O_2CO_3$. *Solid State Sciences* **2014**, *30*, 1–5.

(45) Kumari, L.; Lin, J.-H.; Ma, Y.-R. One-dimensional Bi_2O_3 nanohooks: synthesis, characterization and optical properties. *Journal of Physics: Condensed Matter* **2007**, *19*, 406204.

(46) Dong, W.; Zhu, C. Optical properties of surface-modified Bi_2O_3 nanoparticles. *Journal of Physics and Chemistry of Solids* **2003**, *64*, 265–271.

(47) Zhao, Y.; Shi, H.; Yang, D.; Fan, J.; Hu, X.; Liu, E. Fabrication of a Sb_2MoO_6/g-C_3N_4 Photocatalyst for Enhanced RhB Degradation and H_2 Generation. *The Journal of Physical Chemistry C* **2020**, *124*, 13771–13778.

Graphical TOC Entry

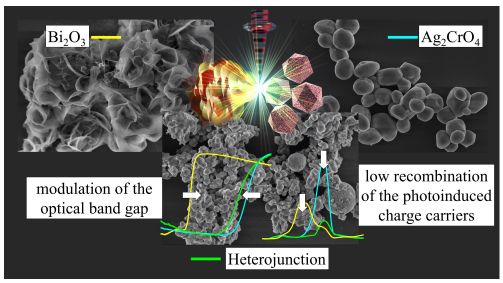

Laser-mediated formation of heterojunction between Ag_2CrO_4 and Bi_2O_3. Its employment enables robust junctions and a reduction in the recombination of photoinduced charge carriers.